RESEARCH ARTICLE | JULY 11 2023

## Unidirectional microwave transduction with chirality selected short-wavelength magnon excitations *⊙*

Yi Li ■ ⑩ ; Tzu-Hsiang Lo ⑩ ; Jinho Lim ⑩ ; John E. Pearson ⑩ ; Ralu Divan ⑩ ; Wei Zhang; Ulrich Welp ⑩ ; Wai-Kwong Kwok ⑩ ; Axel Hoffmann ⑩ ; Valentine Novosad ⑩



Appl. Phys. Lett. 123, 022406 (2023) https://doi.org/10.1063/5.0156369





CrossMark

AIP
Publishing





# Unidirectional microwave transduction with chirality selected short-wavelength magnon excitations

Cite as: Appl. Phys. Lett. **123**, 022406 (2023); doi: 10.1063/5.0156369 Submitted: 28 April 2023 · Accepted: 20 June 2023 · Published Online: 11 July 2023







Yi Li,<sup>1,a)</sup> D Tzu-Hsiang Lo,<sup>2</sup> D Jinho Lim,<sup>2</sup> D John E. Pearson,<sup>1</sup> Ralu Divan,<sup>3</sup> D Wei Zhang,<sup>4</sup> Ulrich Welp,<sup>1</sup> Wai-Kwong Kwok,<sup>1</sup> Axel Hoffmann,<sup>2,b)</sup> D and Valentine Novosad<sup>1,c)</sup>

## **AFFILIATIONS**

- <sup>1</sup>Materials Science Division, Argonne National Laboratory, Lemont, Illinois 60439, USA
- <sup>2</sup>Department of Materials Science and Engineering, UIUC, Urbana, Illinois 61801, USA
- <sup>3</sup>Center for Nanoscale Materials, Argonne National Laboratory, Lemont, Illinois 60439, USA

## **ABSTRACT**

Nonreciprocal magnon propagation has recently become a highly potential approach of developing chip-embedded microwave isolators for advanced information processing. However, it is challenging to achieve large nonreciprocity in miniaturized magnetic thin-film devices because of the difficulty of distinguishing propagating surface spin waves along the opposite directions when the film thickness is small. In this work, we experimentally realize unidirectional microwave transduction with sub-micrometer-wavelength propagating magnons in a yttrium iron garnet (YIG) thin-film delay line. We achieve a non-decaying isolation of 30 dB with a broad field-tunable bandpass frequency range up to 14 GHz. The large isolation is due to the selection of chiral magnetostatic surface spin waves with the Oersted field generated from the coplanar waveguide antenna. Increasing the geometry ratio between the antenna width and YIG thickness drastically reduces the nonreciprocity and introduces additional magnon transmission bands. Our results pave the way for on-chip microwave isolation and tunable delay line with short-wavelength magnonic excitations.

Published under an exclusive license by AIP Publishing. https://doi.org/10.1063/5.0156369

Recent advances in information technologies, such as quantum information, <sup>1</sup> microelectronics, <sup>2</sup> and 5G/6G networks, <sup>3</sup> call for disruptive innovations in microwave signal processing. In particular, circuit-integrated microwave isolators are highly desirable for many applications as they filter unwanted microwave backflow. In quantum information, filtering environmental noise from the output ports is essential for protecting quantum states and entanglement. <sup>4</sup> Being able to embed isolators on chip will significantly reduce the device volume compared to currently used bulk ferrite-based isolators and enable non-Hermitian engineering of dynamic systems at a circuit level. <sup>5,6</sup>

Magnonics offers opportunities for implementing unidirectional microwave transduction with miniaturized geometry.<sup>7–9</sup> Because of their special dispersion relations,<sup>10</sup> magnons support short-wavelength excitations down to nanometer scale at microwave bandwidth<sup>11–16</sup> along with superior frequency tunability with an external magnetic

field. In addition, magnons exhibit nonreciprocity based on many unique properties of magnetic excitations, including intrinsic chirality selection in propagating magnetostatic surface spin waves (MSSW), <sup>17–24</sup> wavevector-dependent spin wave dispersion shifting, <sup>25–37</sup> and non-Hermitian circuit engineering. <sup>38–40</sup> This allows for compact integration of miniaturized, broad-band, and highly tunable isolators in microwave circuits. Furthermore, the realization of miniaturized magnonic isolator is also important for spin wave computing, where magnons are used to carry, transport, and process information. <sup>41,42</sup> Unidirectional flow of magnon information enables the isolation of input and output and ensures deterministic logic output. <sup>43,44</sup>

One major challenge of chip-integrated magnonic microwave isolators is the degradation of nonreciprocity in magnetic thin-film devices. In the past, the dominate mechanism for nonreciprocal spin wave transmission is the asymmetric localization of spin waves at

Department of Physics and Astronomy, University of North Carolina, Chapel Hill, North Carolina 27599, USA

<sup>&</sup>lt;sup>a)</sup>Author to whom correspondence should be addressed: yili@anl.gov

b) Electronic mail: axelh@illinois.edu

c)Electronic mail: novosad@anl.gov

either the top or bottom surface depending on their propagation directions, yielding a large isolation of more than 20 dB.  $^{45,46}$  However, as the film thickness is decreased down to nanometer levels, the surface waves will permeate to the entire thickness and be both excited by antennas at the top surface, leading to suppressed isolation that is typically less than  $10 \, \mathrm{dB}$ . Alternatively, spin wave nonreciprocity can be achieved by chirality selection from well-designed microwave antennas,  $^{22,47,48}$  where +k and -k MSSWs exhibit clockwise and counterclockwise mode profiles depending on the orientation of the magnetization vector, respectively. This technique is not restricted by the film thickness and, thus, can be applied for highly efficient spin wave isolation with the proper geometric design.

In this work, we obtain highly nonreciprocal magnon excitations with over 30 dB isolation in yttrium iron garnet (YIG) thin-film delay lines with a thickness down to 100 nm. The unidirectional magnon transmission can be tuned in a broad frequency range by magnetic field and can reverse the isolation direction as the field direction is reversed. We find the leading mechanism of nonreciprocity to be the Oersted field chirality generated from the coplanar waveguide (CPW) antenna, which selectively couples to the MSSW mode propagating unidirectionally. We also utilize the time-domain functionality of the measurement system to obtain the delay time, group velocity, and pulse linewidth broadening of magnon transmission. Exploring different antenna geometries, we find experimentally that the isolation decreases from 35 to 10 dB as the ratio between the antenna width and YIG thickness increases from 1 to 5. We also find additional magnon transduction bands at large ratios and reveal their nature using the time-domain analysis. The demonstration and physical understanding of high-isolation, high-tunability, and thin-film-based compact microwave isolator are critical for extending microwave engineering with magnonic devices and bring potential for on-chip noise reduction in quantum information applications.

The structure of the delay line is shown in Fig. 1(a). A pair of nanofabricated ground-signal-ground (GSG) CPW antennas is patterned on top of a YIG thin-film stripe with a thickness of  $t_{YIG} = 100$ or 200 nm. The three electrodes of the GSG antennas and the gaps between them have an equal width of w = 200 or 500 nm and a length of 30 µm, leading to the excitation of spin waves with a wavelength of  $\lambda \sim 4w$ , around 800 or 2000 nm. <sup>49,50</sup> The separation of the two CPWs is d = 5, 10, or 20  $\mu$ m. The external magnetic field is applied parallel to the two CPWs in order to define the MSSW propagation modes between the two antennas. Figure 1(b) shows the micromagnetically simulated spatial distribution of the Oersted field  $(h_{rf})$  from the GSG antenna and the mode profiles of the +k and -k MSSW modes for  $t_{\rm YIG} = 100$  nm, w = 200 nm, and  $d = 10 \,\mu{\rm m}$  (see the supplementary material for more descriptions). Note that in Fig. 1(b) the magnetic field and magnetization point into the paper. With this definition, the +k(-k) mode travels from left to right (right to left) in Fig. 1(a). The  $h_{rf}$ profile exhibits a smooth chirality, which matches with the +k mode profile and counter-match with the -k mode profile. Here, the chirality selection is the main mechanism for the experimentally observed large nonreciprocity. Since the spin wave wavelength is still significantly larger than the YIG film thickness, the nonreciprocity due to asymmetric spin wave excitation of the top and bottom surface is much weaker than the chirality-induced nonreciprocity and can be ignored.

Figure 1(c) shows the experimental transmission spectra for the geometry in Fig. 1(b) at  $\mu_0 H_B = 0.22 \,\text{T}$ , which are measured with a

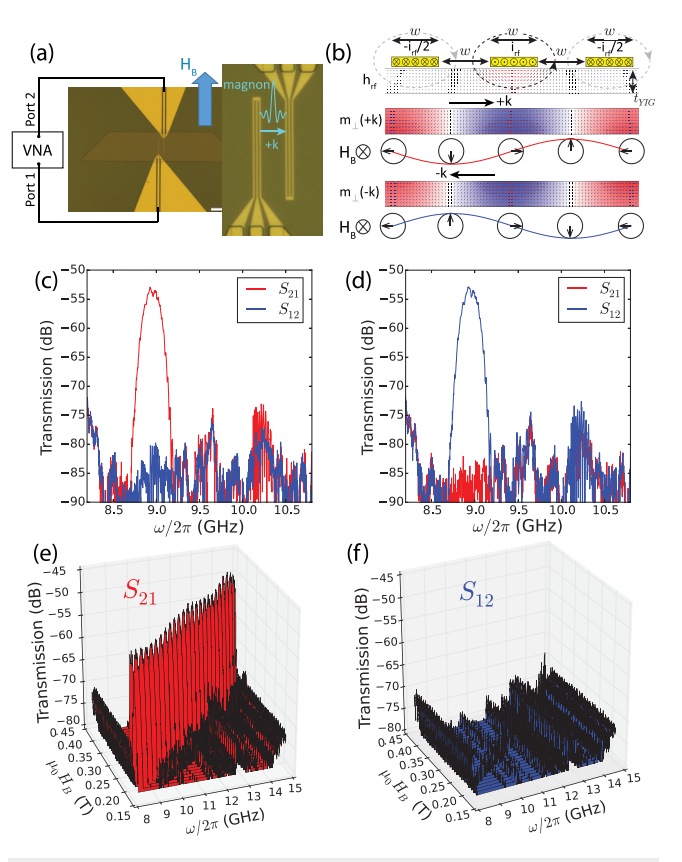


**FIG. 1.** (a) Optical microscope image of the YIG delay line with  $t_{\rm YIG}=100$  nm, w=200 nm, and  $d=10~\mu{\rm m}$ . (b) OOMMF simulations of the top CPW Oersted field chirality and the  $\pm k$  MSSW mode chirality for the geometry in (a). The magnetization vector points into the paper. (c) and (d) Nonreciprocal microwave transmission spectra of the device in (a) at (c)  $\mu_0 H_B=0.22~{\rm T}$  and (d)  $\mu_0 H_B=-0.22~{\rm T}$ . (e) and (f) Repeated measurements of (c) at different magnetic fields, showing a broadband nonreciprocity with a constant isolation of 30 dB.

vector network analyzer (VNA). For magnons that propagate from left to right ( $S_{21}$ ), as shown in Fig. 1(a), a single microwave transmission band is observed around 9 GHz and stands well above the microwave background. By reversing the measurement direction from right to left ( $S_{12}$ ), the transmission band disappears. The  $S_{21}$  band corresponds to the MSSW modes with the wavevector k orthogonal to the magnetization M and from left to right (+k). The magnon isolation direction can also be reversed by flipping the biasing field to  $\mu_0 H_B = -0.22$  T, as shown in Fig. 1(d). With different external biasing fields, the transmission band can be tuned continuously along the frequency axis, as shown in Fig. 1(e). A consistent isolation of 30 dB is measured with negligible change in a broad frequency band from 8 to 15 GHz, as shown in Figs. 1(e) and 1(f).

To examine the performance of the nonreciprocal magnonic delay line in the time domain, we also perform time-domain analysis using the inverse Fast Fourier Transformation (IFFT) function of the VNA. IFFT simulates the input of a sinc function pulse holding an equal weight of all the frequency components set by the frequency window. Figures 2(a) and 2(b) show the frequency and time-domain measurements of the major transmission band ( $S_{21}$ ) with w = 200 and

 $t_{\rm YIG}=100\,$  nm at different antenna separations ( $d=5,\ 10,\$ and  $20\,\mu{\rm m}$ ). For the opposite microwave transmission direction ( $S_{12}$ ), no magnon signals are measured above the noise level. In the frequency domain, nearly identical transmission bands are measured at different d, with only a decreasing transmission amplitude due to the magnon decay with additional propagating distance. In the time domain, the magnon transmission peaks are followed by an initial microwave pulse at 20 ns, which is due to the direct microwave radiation between the two antennas serving as the microwave background in Fig. 2(a). The time delay of the magnon signal from the microwave radiation pulse scales linearly as a function of d, yielding a time delay of 23, 47, and 96 ns at d=5, 10, and 20  $\mu{\rm m}$ , respectively, or a magnon group velocity of  $v_g=217,212$ , and 208 m/s at  $\omega_{\rm peak}/2\pi=10\,{\rm GHz}$ .

The field dependence of the extracted magnon transmission parameters is plotted as a function of peak transmission frequency  $(\omega_{\text{peak}})$  in Figs. 2(c)–2(f). For the frequency domain, all the three devices show nearly frequency-independent peak transmission amplitudes  $(S_{21,\text{peak}})$  and linewidth  $(\Delta\omega_{3dB})$  from 8 to 14 GHz, as shown in Figs. 2(c) and 2(d). The d-dependence of  $S_{21,\text{peak}}$  yields a magnon decay rate of 0.5 dB/ $\mu$ m or an exponential decay length of 8.7  $\mu$ m. The extracted values of  $\Delta\omega_{3dB}/2\pi$  are between 0.1 and 0.15 GHz. Note that it is a function of the GSG antenna geometry and is unrelated to the YIG Gilbert damping. The fluctuation mainly comes from the background noise. For the time domain, the extracted group velocities from time delays [Fig. 2(e)] are consistent for the three devices and show a slow decrease with frequency, which is the characteristic of MSSW modes.

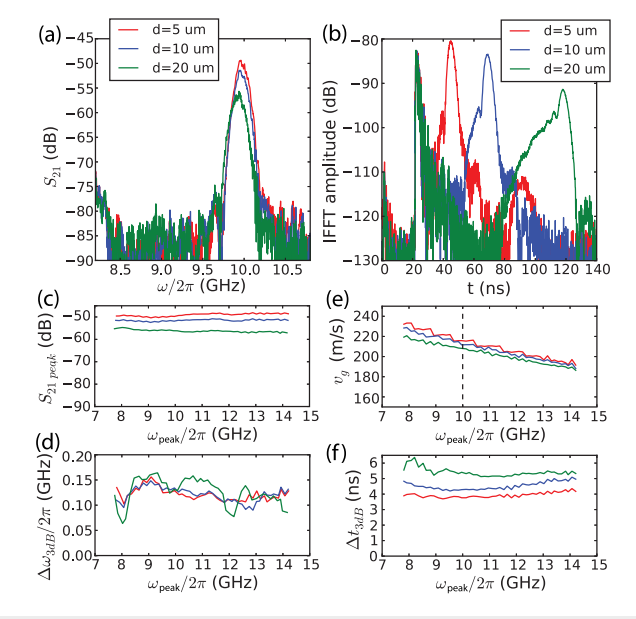


**FIG. 2.** (a) Comparison of microwave transmission spectra with w=200 and  $t_{\rm YIG}=100$  nm, for three different antenna separations d. (b) IFFT of (a) with a transformation window from 3 to 15 GHz. The biasing fields for (a) and (b) are set as  $\mu_0 H_B=0.27$  T. (c) Maximal transmission amplitude  $S_{21,\rm peak}$  as a function of the peak position  $\omega_{\rm peak}$ . (d) 3 dB frequency linewidth  $\Delta\omega_{3dB}$  as a function of  $\omega_{\rm peak}$ . (o) and (d) Extracted from the measurements of (a) at different fields. (e) Group velocity obtained from the magnon time delay and plotted as a function of  $\omega_{\rm peak}$ . The vertical dashed line labels the values obtained at  $\omega_{\rm peak}/2\pi=10$  GHz. (f) 3 dB linewidth of the IFFT peak as a function of  $\omega_{\rm peak}$ . (e) and (f) Extracted from the measurements of (b) at different fields.

IFFT analysis also allows us to access the magnon pulse width  $(\Delta t_{3dB})$ , which is in the range of 4–6 ns for the three devices shown in Fig. 2(f). Because the simulated sinc pulse has a much smaller width (<0.1 ns for a frequency window between 3 and 15 GHz), the measured values of  $\Delta t_{\rm 3dB}$  pose a fundamental limit of the pulse width of the delay line structure. The main source of broadening is the finite spatial width of the antenna for the magnon pulse to pass by. If we take the width of the entire antenna as 4w = 800 nm and the group velocity  $v_{\sigma}$  as 200 m/s, the total traveling time of the magnon pulse across the antenna is  $4w/v_g = 4$  ns, which is close to the lower bound of  $\Delta t_{3\text{dB}}$ . The increase in  $\Delta t_{3\text{dB}}$  with d is due to the distribution of  $v_g$ within the finite bandwidth,  $\Delta\omega_{3dB}$ , leading to the expansion of the magnon wave package as it propagates. As an estimate, the additional magnon pulse broadening  $\Delta t_k$  can be expressed as  $\Delta t_k = (\Delta \omega_{3dB}/\omega)t$ (see the supplementary material for a detailed discussion). From Fig. 2(d),  $\Delta\omega_{3dB}/\omega \approx 1\%$ . This yields  $\Delta t_k \approx 1$  ns by changing d from 5 to 20 nm, which agrees with the change of  $\Delta t_{3dB}$ .

To further explore the role of geometric structure in nonreciprocity, we compare the transmission spectra for a few different antenna geometries with  $d = 10 \,\mu\text{m}$ , with the results shown in Figs. 3(a)–3(c). New sidebands appear that indicate that the geometry coupling of the antenna to the propagating spin wave modes becomes less optimal. For the isolation, we focus on the main mode, marked as mode 1, which corresponds to the wavelength of  $\lambda \sim 4w$ . Experimentally, we see that by increasing w from 200 to 500 nm, there is a major increase in the isolated band  $(S_{12})$  from below the noise background to being clearly visible, leading to a suppressed nonreciprocity. Figure 3(d) summarizes the isolation of mode 1 as a function of antenna-to-YIG aspect ratio,  $w/t_{\rm YIG}$ . The isolation decreases exponentially as  $w/t_{\rm YIG}$ increases. This is mainly because when the YIG film is much thinner than the antenna width, the Oersted field becomes sharply large in the gaps of electrodes, especially at the edges. The large non-sinusoidal component of the spatial Oersted field leads to a finite coupling to the chirality-unfavored propagating spin wave mode and, thus, lowers the

Finally, we use IFFT analysis to identify the nature of additional bands for different antenna geometries in Figs. 3(a)-3(c), which are marked as modes 1, 2, and 3. Figures 3(e)-(h) show the time-domain profiles of different modes for each geometry, including the geometry in Fig. 1(a) as well with the frequency-domain transmission spectrum shown in Fig. 1(c). The frequency windows are limited to the edges of each magnon band in order to filter out the contributions from other bands. Mode 1 is the main transmission band, which contains the main magnon excitation. For mode 2 that appears in Figs. 3(a) and 3(c), the amplitude peak has a longer delay time as compared with mode 1. This supports that mode 2 is the higher harmonic  $(\lambda \sim 4w/3)$  because for MSSW modes, the  $\omega$ -k dispersion curve softens at higher k, and the group velocity becomes smaller, resulting in longer travel time of propagating magnons. Mode 3 appearing in Figs. 3(b) and 3(c) exhibits a long time span starting from t = 40 ns and extending beyond t = 100 ns. We deduce that mode 3 is the obliquely launched backward-volume magnetostatic spin waves (BVMSWs) with canted wavevector due to spin wave diffraction.<sup>51,52</sup> Our micromagnetic simulations confirm that modes 1 and 2 correspond to the  $\lambda \sim 4w$  and 4w/3 modes, respectively (see the supplementary material). We do not observe the excitation of mode 3 in the simulation, which suggests that it is related to the CPW antenna geometry with a

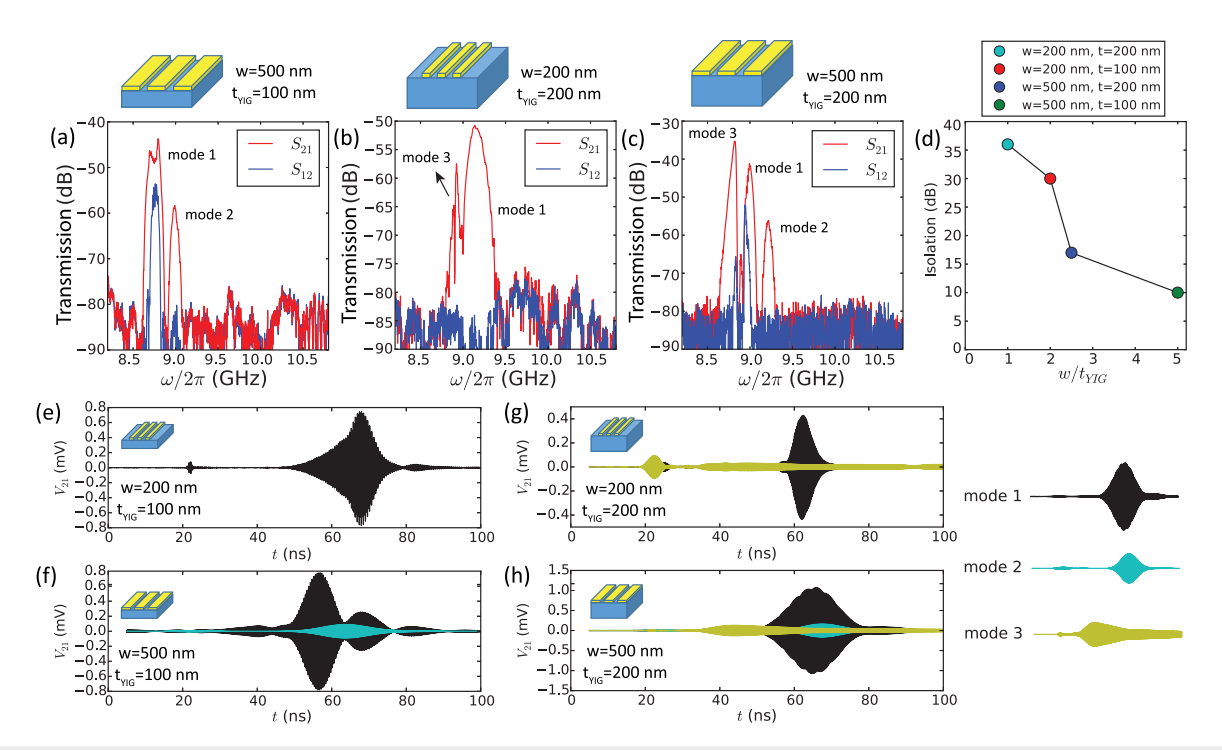


FIG. 3. (a)–(c) Nonreciprocal microwave transmission spectra with different geometries: (a) w=500 and  $t_{\rm YIG}=100$  nm; (b) w=200 and  $t_{\rm YIG}=200$  nm; and (c) w=500 and  $t_{\rm YIG}=200$  nm. The biasing fields are all  $\mu_0 H_B=0.22\,\rm T$  for comparison. (d) Summary of experimental magnon isolations as a function of aspect ratio  $w/t_{\rm YIG}$ . (e)–(h) Decomposition of magnonic mode traces from IFFT of the frequency domain spectra at  $\mu_0 H_B=0.22\,\rm T$ . (e) Converted from IFFT of Fig. 1(c). (f)–(h) Converted from IFFT of Figs. 3(a)–3(c), respectively. The amplitudes are measured in voltage ( $V_{21}$ ).

finite length in the design. From the phase analysis measured by VNA, the high-frequency edge of mode 3 exhibits a near-zero group velocity due to the flat  $\omega$ -k dispersion, causing the magnon pulse to take long time to be transmitted. Sa-55 We conclude from the time-domain analysis that purer magnon modes arise from narrower GSG antenna widths, which is desirable for minimizing loss and decoherence during the pulse microwave processing with the nonreciprocal magnon delay line.

In summary, we present a systematic study of YIG-thin-film magnon delay lines with broad-band isolation above 30 dB. We identify the source of nonreciprocity as the selective coupling of the chiral Oersted field from the GSG antenna to the propagating MSSW modes in only one direction. Using time-domain IFFT analysis, we determine important parameters of the delay line, including time delay, group velocity, bandwidth, and time-domain broadening. We also identify the nature of the additional magnon transmission bands as the higher harmonic and the canted BVMSWs band, which can be suppressed by reducing the aspect ratio of the antenna and the YIG thickness. Our results show promise of nonreciprocal magnonic delay lines for processing pulse microwave signals with excellent noise isolation, which may be implemented as chip-embedded microwave isolators for spin wave computing and quantum information processing. We note that our demonstration of nonreciprocal spin wave propagation can also be combined with the recent work of spin-torque spin wave amplification 56,57 for implementing unidirectional magnonic microwave nano-amplifiers.

See the supplementary material for the description of OOMMF simulations, Oersted field distribution vs antenna-film aspect ratio,  $S_{11}$ 

measurements, derivation of IFFT pulse width broadening  $\Delta\omega_{3dB}$  by group velocity dispersion  $\Delta v_g$ , and micromagnetic simulations of mode profiles of new sidebands.<sup>51</sup>

This work was supported by the U.S. DOE, Office of Science, Basic Energy Sciences, Materials Sciences and Engineering Division, with parts of the manuscript preparation, first-principle calculations, device design, and sample fabrication and characterization supported under Contract No. DE-SC0022060. U.W., W.-K.K., and V.N. acknowledge the support by the U.S. DOE, Office of Science, Basic Energy Sciences, Materials Sciences and Engineering Division. Use of the Center for Nanoscale Materials (CNM), an Office of Science user facility, was supported by the U.S. Department of Energy, Office of Science, Office of Basic Energy Sciences, under Contract No. DE-AC02-06CH11357. W.Z. acknowledges support by the US National Science Foundation under Contract No. NSF-ECCS 2246254. We acknowledge Jiang-Chao Qian, Zhihao Jiang, Andre Schleife, Wolfgang Pfaff, and Jian-Min Zuo from UIUC for their helpful discussions.

## AUTHOR DECLARATIONS Conflict of Interest

The authors have no conflicts to disclose.

## **Author Contributions**

Yi Li: Conceptualization (equal); Data curation (equal); Formal analysis (equal); Funding acquisition (equal); Investigation (equal); Methodology (equal); Project administration (equal); Resources

(equal); Software (equal); Supervision (equal); Validation (equal); Visualization (equal); Writing – original draft (equal); Writing – review & editing (equal). Valentine Novosad: Conceptualization (equal); Data curation (equal); Funding acquisition (equal); Investigation (equal); Supervision (equal); Writing – review & editing (equal). Tzu-Hsiang Lo: Data curation (equal); Formal analysis (equal); Software (equal). Jinho Lim: Data curation (equal); Formal analysis (equal); Software (equal). John E. Pearson: Data curation (equal); Methodology (equal). Ralu Divan: Methodology (equal); Resources (equal). Wei Zhang: Conceptualization (equal); Writing – review & editing (equal). Ulrich Welp: Data curation (equal); Methodology (equal); Resources (equal); Supervision (equal). Wai-Kwong Kwok: Funding acquisition (equal); Supervision (equal). Axel Hoffmann: Conceptualization (equal); Funding acquisition (equal); Investigation (equal); Supervision (equal); Investigation (equal); Investigatio

#### **DATA AVAILABILITY**

The data that support the findings of this study are available from the corresponding author upon reasonable request.

## REFERENCES

- <sup>1</sup>A. Blais, A. L. Grimsmo, S. M. Girvin, and A. Wallraff, Rev. Mod. Phys. 93, 025005 (2021).
- <sup>2</sup>B. Razavi, Fundamentals of Microelectronics (Wiley, London, 2013).
- <sup>3</sup>N. Al-Falahy and O. Alani, IEEE IT Prof. **19**, 12 (2017).
- <sup>4</sup>D. Suter and G. A. Álvarez, Rev. Mod. Phys. 88, 041001 (2016).
- <sup>5</sup>R. El-Ganainy, K. G. Makris, M. Khajavikhan, Z. H. Musslimani, S. Rotter, and D. N. Christodoulides, Nat. Phys. 14, 11 (2018).
- <sup>6</sup>H. M. Hurst and B. Flebus, arXiv:2209.03946 (2022).
- <sup>7</sup>V. G. Harris, A. Geiler, Y. Chen, S. D. Yoon, W. M. A. Yang, Z. Chen, P. He, P. V. Parimi, X. Zuo, C. E. Patton, M. Abe, O. Acher, and C. Vittoria, J. Magn. Magn. Mater. 321, 2035 (2009).
- <sup>8</sup>A. A. Serga, A. V. Chumak, and B. Hillebrands, J. Phys. D: Appl. Phys. 43, 264002 (2010).
- <sup>9</sup>A. Barman, G. Gubbiotti, S. Ladak *et al.*, J. Phys.: Condens. Matter **33**, 413001 (2021).
- 10 C. Herring and C. Kittel, Phys. Rev. **81**, 869 (1951).
- C. Liu, J. Chen, T. Liu, F. Heimbach, H. Yu et al., Nat. Commun. 9, 738 (2018).
   Y. Shiota, T. Taniguchi, M. Ishibashi, T. Moriyama, and T. Ono, Phys. Rev. Lett. 125, 017203 (2020).
- <sup>13</sup>B. Heinz, T. Brächer, M. Schneider, Q. Wang, B. Lägel, A. M. Friedel, D. Breitbach, S. Steinert, T. Meyer, M. Kewenig, C. Dubs, P. Pirro, and A. V. Chumak, Nano. Lett. 20, 4220 (2020).
- <sup>14</sup>K. Baumgaertl, J. Gräfe, P. Che, A. Mucchietto, J. Förster, N. Träger, M. Bechtel, M. Weigand, G. Schütz, and D. Grundler, Nano. Lett. 20, 7281 (2020).
- <sup>15</sup>H. Wang, L. Flacke, W. Wei, S. Liu, H. Jia, J. Chen, L. Sheng, J. Zhang, M. Zhao, C. Guo, C. Fang, X. Han, D. Yu, M. Althammer, M. Weiler, and H. Yu, Appl. Phys. Lett. 119, 152402 (2021).
- 16P. Che, K. Baumgaertl, A. Kúkoľová, C. Dubs, and D. Grundler, Nat. Commun. 11, 1445 (2022).
- <sup>17</sup>P. Khalili Amiri, B. Rejaei, M. Vroubel, and Y. Zhuaang, Appl. Phys. Lett. **91**, 062502 (2007).
- <sup>18</sup>T. Schneider, A. A. Serga, T. Neumann, B. Hillebrands, and M. P. Kostylev, Phys. Rev. B 77, 214411 (2008).
- <sup>19</sup>K. Sekiguchi, K. Yamada, S. M. Seo, K. J. Lee, D. Chiba, K. Kobayashi, and T. Ono, Appl. Phys. Lett. **97**, 022508 (2010).
- <sup>20</sup> M. Jamali, J. H. Kwon, S.-M. Seo, K.-J. Lee, and H. Yang, Sci. Rep. 3, 3160 (2013).
- <sup>21</sup>K. L. Wong, L. Bi, M. Bao, Q. Wen, J. P. Chatelon, Y.-T. Lin, C. A. Ross, H. Zhang, and K. L. Wang, Appl. Phys. Lett. **105**, 232403 (2014).
- <sup>22</sup>P. Deorani, J. H. Kwon, and H. Yang, Curr. Appl. Phys. **14**, S129 (2014).
- <sup>23</sup>M. Nakayama, K. Yamanoi, S. Kasai, S. Mitani, and T. Manago, Jpn. J. Appl. Phys., Part 1 54, 083002 (2015).

- <sup>24</sup>K. Shibata, K. Kasahara, K. Nakayama, V. V. Kruglyak, M. M. Aziz, and T. Manago, J. Appl. Phys. **124**, 243901 (2018).
- 25 J.-H. Moon, S.-M. Seo, K.-J. Lee, K.-W. Kim, J. Ryu, H.-W. Lee, R. D. McMichael, and M. D. Stiles, Phys. Rev. B 88, 184404 (2013).
- <sup>26</sup>H. T. Nembach, J. M. Shaw, M. Weiler, E. Jue, and T. J. Silva, Nat. Phys. 11, 825 (2015).
- <sup>27</sup>J. Lan, W. Yu, R. Wu, and J. Xiao, Phys. Rev. X 5, 041049 (2015).
- 28]. M. Lee, C. Jang, B.-C. Min, S.-W. Lee, K.-J. Lee, and J. Chang, Nano Lett. 16, 62 (2016).
- <sup>29</sup>T. Brächer, O. Boulle, G. Gaudin, and P. Pirro, Phys. Rev. B 95, 064429 (2017).
   <sup>30</sup>R. Gallardo, T. Schneider, A. Chaurasiya, A. Oelschlägel, S. Arekapudi, A. Roldán-Molina, R. Hübner, K. Lenz, A. Barman, J. Fassbender, J. Lindner, O. Hellwig, and P. Landeros, Phys. Rev. Appl. 12, 034012 (2019).
- <sup>31</sup>R. Verba, V. Tiberkevich, and A. Slavin, Phys. Rev. Appl. 12, 054061 (2019).
- <sup>32</sup>J. Chen, T. Yu, C. Liu, T. Liu, M. Madami, K. Shen, J. Zhang, S. Tu, M. S. Alam, K. Xia, M. Wu, G. Gubbiotti, Y. M. Blanter, G. E. W. Bauer, and H. Yu, Phys. Rev. B **100**, 104427 (2019).
- <sup>33</sup>H. Wang, J. Chen, T. Liu, J. Zhang, K. Baumgaertl, C. Guo, Y. Li, C. Liu, P. Che, S. Tu, S. Liu, P. Gao, X. Han, D. Yu, M. Wu, D. Grundler, and H. Yu, Phys. Rev. Lett. **124**, 027203 (2020).
- 34M. Ishibashi, Y. Shiota, T. Li, S. Funada, T. Moriyama, and T. Ono, Sci. Adv. 6, eaaz6931 (2020).
- 35M. Xu, K. Yamamoto, J. Puebla, K. Baumgaertl, B. Rana, K. Miura, H. Takahashi, D. Grundler, S. Maekawa, and Y. Otani, Sci. Adv. 6, eabb1724 (2020).
- <sup>36</sup>P. J. Shah, D. A. Bas, I. Lisenkov, A. Matyushov, N. X. Sun, and M. R. Page, Sci. Adv. 6, eabc5648 (2020).
- <sup>37</sup>J. Han, Y. Fan, B. C. McGoldrick, J. Finley, J. T. Hou, P. Zhang, and L. Liu, Nano Lett. 21, 7037 (2021).
- 38Y.-P. Wang, J. W. Rao, Y. Yang, P.-C. Xu, Y. S. Gui, B. M. Yao, J. Q. You, and C.-M. Hu, Phys. Rev. Lett. 123, 127202 (2019).
- 39 X. Zhang, A. Galda, X. Han, D. Jin, and V. M. Vinokur, Phys. Rev. Appl. 13, 044039 (2020).
- <sup>40</sup>Y.-Y. Wang, S. van Geldern, T. Connolly, Y.-X. Wang, A. Shilcusky, A. McDonald, A. A. Clerk, and C. Wang, Phys. Rev. Appl. 16, 064066 (2021).
- 41 A. V. Chumak, V. I. Vasyuchka, A. A. Serga, and B. Hillebrands, Nat. Phys. 11, 453 (2015).
- <sup>42</sup>A. Mahmoud, F. Ciubotaru, F. Vanderveken, A. V. Chumak, S. Hamdioui, C. Adelmann, and S. Cotofana, J. Appl. Phys. 128, 161101 (2020).
- 43 N. Sato, K. Sekiguchi, and Y. Nozaki, Appl. Phys. Express **6**, 063001 (2013).
- <sup>44</sup>G. Talmelli, T. Devolder, N. Träger, J. Förster, S. Wintz, M. Weigand, H. Stoll, M. Heyns, G. Schütz, I. P. Radu, J. Gräfe, F. Ciubotaru, and C. Adelmann, Sci. Adv. 6, eabb4042 (2020).
- <sup>45</sup>M. R. Daniel, J. Appl. Phys. 48, 1732 (1977).
- <sup>46</sup>R. Camley, Surf. Sci. Rep. 7, 103 (1987).
- <sup>47</sup>Y. Au, E. Ahmad, O. Dmytriiev, M. Dvornik, T. Davison, and V. V. Kruglyak, Appl. Phys. Lett. 100, 182404 (2012).
- 48 V. V. Kruglyak, Appl. Phys. Lett. 119, 200502 (2021).
- <sup>49</sup>M. Sushruth, M. Grassi, K. Ait-Oukaci, D. Stoeffler, Y. Henry, D. Lacour, M. Hehn, U. Bhaskar, M. Bailleul, T. Devolder, and J.-P. Adam, Phys. Rev. Res. 2, 043203 (2020).
- <sup>50</sup>T. Devolder, G. Talmelli, S. M. Ngom, F. Ciubotaru, C. Adelmann, and C. Chappert, Phys. Rev. B 103, 214431 (1021).
- 51 J. Stigloher, M. Decker, H. S. Körner, K. Tanabe, T. Moriyama, T. Taniguchi, H. Hata, M. Madami, G. Gubbiotti, K. Kobayashi, T. Ono, and C. H. Back, Phys. Rev. Lett. 117, 037204 (2016).
- <sup>52</sup>V. Vlaminck, L. Temdie, V. Castel, M. Jungfleisch, D. Stoeffler, Y. Henry, and M. Bailleul, J. Appl. Phys. **133**, 053903 (2023).
- <sup>53</sup>M. Chen, M. A. Tsankov, J. M. Nash, and C. E. Patton, Phys. Rev. B 49, 12773 (1994).
- 54S. Demokritov, B. Hillebrands, and A. Slavin, Phys. Rep. 348, 441 (2001).
- <sup>55</sup>A. V. Chumak, A. A. Serga, S. Wolff, B. Hillebrands, and M. P. Kostylev, Appl. Phys. Lett. **94**, 172511 (2009).
- <sup>56</sup>D. Breitbach, M. Schneider, F. Kohl, L. Scheuer, B. Heinz, R. O. Serha, J. Maskill, T. Brächer, B. Lägel, C. Dubs, V. S. Tiberkevich, A. N. Slavin, A. A. Serga, B. Hillebrands, A. V. Chumak, and P. Pirro, arXiv:2208.11455 (2022).
- <sup>57</sup>H. Merbouche, B. Divinskiy, D. Gouéré, R. Lebrun, A. El-Kanj, V. Cros, P. Bortolotti, A. Anane, S. O. Demokritov, and V. E. Demidov, arXiv:2303.04695 (2023).